Electrical and optical characterization of CdTe solar cells with CdS and CdSe buffers—A comparative study

Md Dalim Mia,[1] Craig H. Swartz,[1] Sanjoy Paul,[1] Sandeep Sohal,[1] Corey R. Grice,[2] Yanfa Yan,[2] Mark Holtz,[1] and Jian V. Li[3,a)]

[1]*Materials Science, Engineering, and Commercialization (MSEC) Program, Department of Physics, Texas State University, San Marcos, Texas 78666*

[2]*Department of Physics and Astronomy, The University of Toledo, Toledo, Ohio 43606*

[3]*Department of Aeronautics and Astronautics, National Cheng Kung University, Tainan 70101, Taiwan*

(Received 12 June 2018; accepted 21 August 2018; published 5 September 2018)

A study is reported comparing the electrical and optical properties of CdTe solar cells, prepared using CdS and CdSe buffer layers, to investigate defects in the bulk and interface, carrier transport, and recombination. Temperature dependent capacitance–voltage measurement and admittance spectroscopy were used to extract carrier concentration, resistivity, charge carrier mobility, and their temperature dependence. The authors identify the presence of two defect signatures corresponding to carrier freeze-out and the formation of a Schottky back-contact barrier. The back-contact barrier height (≈300 meV) extracted from the temperature dependent current density–voltage (JVT) experiment was confirmed by conventional admittance spectroscopy. The activation energies of mobility (resistivity) are 101.2 ± 2.5 meV (92.6 ± 2.3 meV) and 84.7 ± 2.7 meV (77.6 ± 4.5 meV) for CdS and CdSe buffer layers, respectively. Intensity dependent photoluminescence analysis demonstrates that the CdSe/CdTe device exhibits lower radiative efficiency than the CdS/CdTe device. This confirms the presence of higher defects in the CdSe/CdTe device corroborated by temperature dependent V_{OC} analysis. The comparative electrical and optical analysis provides insight into improving the performance of CdTe solar cell device by selenization. *Published by the AVS.*
https://doi.org/10.1116/1.5044219

I. INTRODUCTION

The polycrystalline CdTe-based thin-film photovoltaic (PV) cell is one of the most promising technologies for solar energy conversion because of its low fabrication cost, high efficiency, reliability, and stability.[1–4] This is the only commercially available thin-film technology in solar energy conversion with lower costs than the conventional silicon technology. The record efficiency to date is $22.1 \pm 0.5\%$.[5] Significant efforts on multiple fronts have aimed to further improve the CdTe efficiency. In Cu(In,Ga)Se_2 solar cells, bandgap engineering of the absorber layer through alloying has proven successful when producing a graded bandgap in comparison with the uniform bandgap $CuInSe_2$ technology.[6,7] These successes suggest that bandgap engineering of the absorber layer in CdTe devices, e.g., via selenization, may lead to improvements in this technology.

Compared with the standard CdS/CdTe solar cell, it has been found that CdSe/CdTe cells show an enhanced photoresponse in the short- and long-wavelength regimes and enhancement of the short-circuit current (J_{SC}).[8] The higher solubility and stronger interdiffusion of Se through the CdTe absorber, when compared with S, leads to $CdTe_xSe_{1-x}$ alloy formation.[9,10] The composition, structure, morphology, and photoactivity in the $CdTe_xSe_{1-x}$ alloy have also been investigated with various degrees of Se diffusion.[8] Although higher photo-response and J_{SC} were observed in the CdSe/CdTe device, it suffers notable open-circuit voltage (V_{OC}) loss.[9–12] This voltage limitation may be due to defects, bulk recombination, interface recombination, and nonohmic back-contact potential barrier. To identify and address these issues, combined electrical and optical characterization is necessary.

Electrical transport study of the carrier mobility and resistivity, along with their temperature dependence, is also important for further improving device quality and hence efficiency. Electrical transport is conventionally studied using Hall[12,13] and pulsed laser time-of-flight photo-transient measurement[14–16] which imposes some restrictions. For example, transport study via Hall measurements is at the material level and challenging with low carrier concentration. Time-of-flight, on the other hand, is difficult when working with thin absorber films and the presence of an n^+-p junction. In comparison, capacitance–voltage (CV) and admittance spectroscopy (AS) measurements are relatively simple and, more importantly, applicable to solar cell devices.[17–20] AS is also effective for understanding semiconductor defects and their energetic location, and their correlation with the charge transport phenomena in PV devices.[20] Combined temperature and intensity dependent photoluminescence (PL) studies are well established for yielding valuable information on defects and radiative recombination.[21–24]

We report a comparative study of electrical and optical properties of CdTe solar cells fabricated using two different buffer layers, CdS and CdSe. Temperature dependent CV and AS studies were conducted to understand the charge transport properties in these devices. We also performed the temperature dependent dark current–voltage (JVT) measurement to estimate the back-contact barrier height which is one

a)Electronic mail: jianvli@mail.ncku.edu.tw

TABLE I. Summary results for the electrical and optical characterization of CdTe solar cells with CdS and CdSe buffers.

Buffer	V_{OC} (V)	J_{SC} (mA/cm^2)	FF (%)	η (%)	Absorber thickness (μm)	Defect carrier freeze-out (meV)	Defect back-contact (meV)	$E_{a,\mu}$ (meV)	$E_{a,\rho}$ (meV)	φ_{bc} (meV)	E_a (eV)	E_g (eV)
CdS	0.847	24.7	70.0	14.6	3.88	107 ± 4.5	304.2 ± 3.6	101.2 ± 2.5	92.6 ± 3.3	294.6 ± 5.1	1.38	1.46
CdSe	0.690	26.9	64.8	12.1	5.23	90.8 ± 2.2	321.5 ± 8.6	84.7 ± 2.7	77.6 ± 4.5	329.4 ± 8.3	1.29	1.4

of the key issues in CdTe devices. Using drive-level capacitance profiling (DLCP), we also study defects present in these devices. Combined V_{OC} analysis and intensity dependent photoluminescence (PL-I) studies are used to understand the nonradiative and radiative recombination, respectively. Our experimental observations aim to provide information to better understand the role of CdS and CdSe buffer layers in CdTe solar cells and further their technological development.

II. SAMPLE PREPARATION

The CdTe solar cell samples with CdS and CdSe buffer layers were prepared with solar cell parameters summarized in Table I. The layer sequences are soda lime glass/SnO_2:F/SnO_2/CdS and CdSe buffer/CdTe absorber/Cu-Au back-contact.[25,26] Schematics of the device stacks are shown in Fig. 1. Both CdS and CdSe buffer layers used in this study were deposited by radio frequency magnetron sputtering. CdTe layers (thickness ~4 μm) were grown at 607 °C substrate temperature by close space sublimation using 5*N* purity source materials (Materion). $CdCl_2$ postdeposition annealing treatment was carried out for 30 min at 390 °C in dry air ambience, with a saturated solution of $CdCl_2$ in methanol applied to the CdTe surface. After cooling to room temperature, the thin-film samples were rinsed with methanol and transferred into a thermal evaporator for back-contact deposition, without pursuing any chemical treatment step. The back-contact consisting of thermally evaporated Cu (4 nm)/Au (40 nm) bilayer using a shadow mask containing 20 dots (each with an area of 0.08 cm^2) was used. The devices were subsequently annealed at 200 °C for 20 min in N_2 ambience to facilitate Cu diffusion.

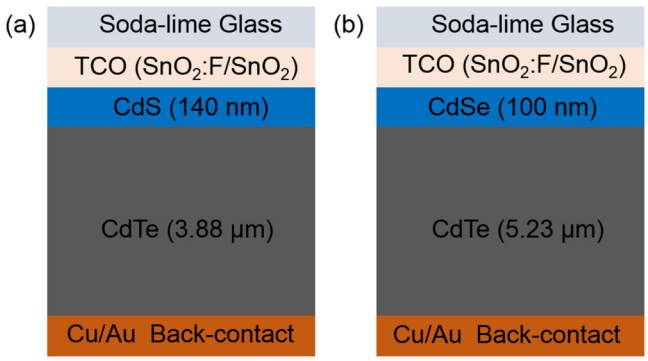

FIG. 1. Schematic of the CdTe device stacks with CdS and CdSe buffers.

III. EXPERIMENT

We performed DC measurements using a Keysight B2912A source measure unit and AC measurements (i.e., *C*–*V* and AS) with a Keysight E4990A impedance analyzer. In the AS measurements, the frequency sweep was from 1 kHz to 1 MHz and the AC modulation amplitude was 35 mV_{rms}; DC bias was varied from −0.6 to 1.6 V. In DLCP measurements, the AC modulation amplitude was varied from 15 to 215 mV_{rms}. A helium closed-cycle cryogenic system was used to carry out all the temperature dependent measurements ranging from 50 to 350 K with step 10 K. For light JVT measurements, a light source equivalent to AM1.5 was used. For the PL measurements, we used an argon ion laser with a photon energy of 2.41 eV as excitation at modulation frequency 400 Hz. A 6.5× objective lens focused the laser light to give a 120-μm full-width-at-half-maximum spot on the sample. Absolute excitation power was measured at the sample position using a calibrated power meter. The PL was collected through the same objective, passed through optical filters to reject reflected laser light, and detected by a photomultiplier tube. PL intensity was recorded as the laser intensity was changed over six orders of magnitude using a series of calibrated neutral density filters. Spectral PL was also performed with excitation photon energy 1.59 eV.

IV. RESULTS AND DISCUSSION

In exploring the comparative electrical properties in CdTe solar cells with CdS and CdSe buffers, we first study the carrier density using CV measurement and DLCP techniques. The profiling serves to estimate the carrier density at different temperatures and provide information about the presence of defects in the absorber layers. Acceptor density (N_a) profiles by these two methods—CV (red) and DLCP (blue)—are shown in Fig. 2(a) for the CdTe device prepared with CdS

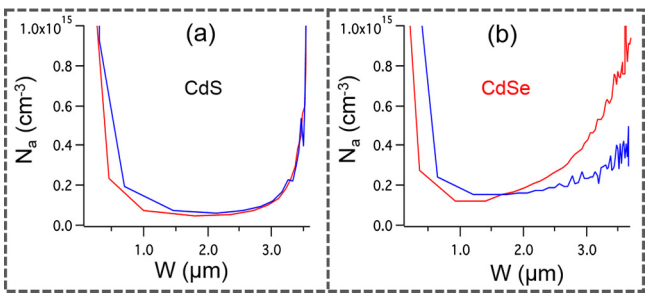

FIG. 2. Experimental carrier density profiles in CdTe solar cells with CdS (a) and CdSe (b) using CV (gray) and DLCP (black) method.

buffer and Fig. 2(b) for the CdSe buffer. For the CdS-buffered sample, the CV profile matches well with the DLCP profile, which can be due to negligible bulk defects contributing to the CV measurements. However, in the case of CdSe buffer, an apparent dissimilarity was observed between the two profiles. We attribute the dissimilarity to the presence of bulk defects and highly graded bandgap, which may result in a spatial variation of the defect level energy.[27,28] The increase of the apparent carrier density obtained from the CV profile data is due to the electrostatic contribution from a significant concentration of the deep level defects.[27,29]

In the depletion region, band bending under a reverse bias enlarges the separation between the valence band and the Fermi level E_F, which causes deep levels in the front portion of the depletion region to drop below E_F. Hence, deep levels are filled by electrons thereby contributing to the space charge. Because of this, the apparent carrier density (N_a) extracted by the simple CV method is greater than the actual N_a. Under forward bias, the back-contact junction becomes reverse biased for both CdTe/CdSe and CdTe/CdS, which limits the current flow, introducing a well-known rollover feature at large forward bias in the dark JVT curve. Under large forward bias, the back-contact shares both DC and AC modulation with the front junction, consequently reducing the overall capacitance of the device and contributing to the apparent increase of N_a in the CV and DLCP profile, forming the characteristic U shape[29,30] seen in Fig. 2.

Figure 3 shows the differential capacitance spectra (from AS data) with distinct minima corresponding to the signatures of two defects. The corresponding activation energies indicated are determined from the Arrhenius analysis of the admittance peak frequency ω_P shown in Fig. 4. These are (107.4 ± 4.5 meV and 304.2 ± 3.6 meV) and (90.8 ± 2.2 meV and 321.5 ± 8.6 meV) for CdTe/CdS and CdTe/CdSe devices, respectively. The lower activation energies are attributed to the freeze-out of CdTe absorber conductivity.[20] On the other hand, the higher activation energy is likely indicative of the potential barrier height of the back contact.[9,31] We verify this below by estimating the back-contact barrier heights in both cells using JVT measurements under dark conditions.

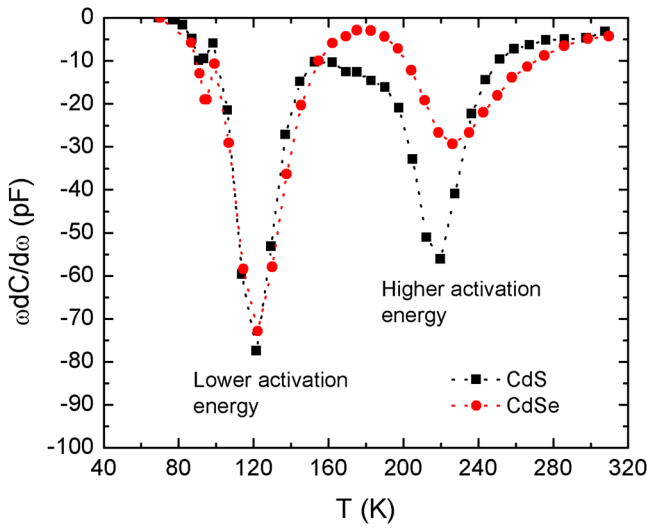

FIG. 3. Differential capacitance spectra (the representation is at $\omega = 6.28 \times 10^5$ Hz and $V = 0$ V) for CdTe solar cells with two different buffers (CdS and CdSe) showing two peaks which lead to two different activation energies. The signature of lower activation energy is due to freeze-out of the CdTe absorber, whereas the signature of higher activation energy is associated with the back-contact potential barrier height.

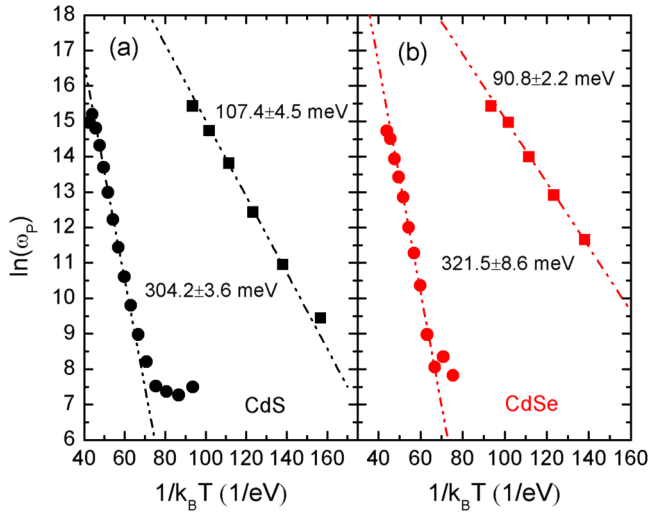

FIG. 4. $\ln(\omega_P)$ vs $1/k_BT$ plot to estimate the activation energy of defects at zero bias (using the Fig. 3 data at different temperature) for CdS/CdTe and CdSe/CdTe devices.

We explore the hole carrier transport in both types of solar cells which involves the admittance measurement of the entire n-CdS/p-CdTe and n-CdSe/p-CdTe solar cells as a function of angular frequency ω ($\omega = 2\pi f$, f = linear frequency) and temperature (T). The response of the majority carrier to the frequency of the AC signal in AS measurement is limited by the modified dielectric relaxation frequency ($\omega_{mdr} = W/t\varepsilon\rho$), where ρ and ε are the material resistivity and permittivity, respectively, W is the depletion width, and t is the absorber thickness. For $\omega < \omega_{mdr}$, the absorber in the quasineutral region behaves as a conductor with a bulk conductance of $A/\rho(t - W)$, A is the device area. For $\omega > \omega_{mdr}$, the quasineutral absorber behaves like a capacitor with a bulk capacitance of $\varepsilon A/(t - W)$. Here, our main aim is to extract the resistivity and mobility of hole carrier and the temperature dependence. A detailed discussion of the AS technique and corresponding theory can be found elsewhere.[18,32]

The frequency dependent capacitance response (C vs f, not shown here) shows a step transition with an inflection frequency which is the modified dielectric relaxation frequency $\omega_{mdr} = (W/t)(1/\rho\varepsilon)$ which can also be seen in the minimal point in the frequency dependent differential capacitance ($\omega dC/d\omega$ vs $\omega/2\pi$). The application of DC bias (V) changes the depletion width according to $W = \sqrt{(2\varepsilon\,(V_{bi} - V))/qN_a}$, meaning ω_{mdr} depends on V. Here, q is the elementary charge and V_{bi} is the built-in potential. The bias dependent square of ω^2_{mdr} in the n^+-p junction (CdS or CdSe/CdTe) is given by

$$\omega^2_{mdr} = \frac{2}{q\varepsilon N_a \rho^2 t^2}(V_{bi} - V) \quad (1)$$

so that ω_{mdr}^2 depends linearly on V. Bias dependent AS measurement therefore enables the extraction of resistivity ρ and carrier mobility μ $(=1/N_a q\rho)$ from the slope $2/q\varepsilon N_a\rho^2 t^2$, i.e., $\rho = \sqrt{2/(q\varepsilon t^2 N_a \times Slope)}$ and $\mu = \sqrt{(\varepsilon t^2 \times Slope)/2qN_a}$ with known absorber thickness t. We estimate temperature dependent N_a from temperature dependent CV measurement described below.

Differential capacitance spectra (at $T = 104$ K) with bias varied from -0.3 to $+0.3$ V, in $\Delta V = 0.1$ V steps for the CdS-buffered and CdSe-buffered cells are shown in Figs. 5(a) and 5(b), respectively, from which bias dependent ω_{mdr} were measured. Corresponding linear dependence of ω_{mdr}^2 with V is shown in Figs. 5(c) and 5(d). Using Eq. (1) and the slopes $1.89 \times 10^{12}\ s^{-2}\ V^{-1}$ (CdS) and $3.26 \times 10^{12}\ s^{-2}\ V^{-1}$ (CdSe), respectively, we extract the resistivity and hole mobility. The values obtained from this analysis are $\rho = (4.04 \pm 0.88) \times 10^5\ \Omega$ cm and $\mu = (3.79 \pm 0.83) \times 10^{-2}$ cm^2/V s (CdS buffer) and $\rho = (2.05 \pm 0.53) \times 10^5\ \Omega$ cm and $\mu = (7.28 \pm 0.19) \times 10^{-2}$ cm^2/V s (CdSe buffer) at $T = 104$ K. Here, in this estimation, we have used the carrier concentrations indicated in Figs. 5(c) and 5(d) and estimated from the temperature dependent CV profiling as shown in Fig. 6. The permittivity for CdTe used in our calculation is $\varepsilon = 10.3\varepsilon_0$.[33]

The thickness of the absorber used in our resistivity and mobility calculation (in both CdTe/CdS and CdTe/CdSe cells) was estimated from the low-temperature range of depletion width results, shown in Fig. 7, which were obtained from the temperature dependent C–V data. The absorber thickness for CdS/CdTe and CdTe/CdSe devices was taken from the fully depleted regime ($T < 100$ K) and their values are 3.88 and 5.23 μm, respectively.

Figure 8 shows the temperature dependence of hole mobility and resistivity in the CdTe devices in the range 74–124 K. With increasing temperature, the mobility increases with the expected concomitant decrease in resistivity. The mobility and resistivity of the CdS/CdTe device vary between μ: $(4.44 \pm 0.77) \times 10^{-4}$ cm^2/V s and (0.22 ± 0.03) cm^2/V s and ρ: $(1.37 \pm 0.24) \times 10^7\ \Omega$ cm and $(0.92 \pm 0.14) \times 10^5\ \Omega$ cm in the temperature range 74–124 K. In the same temperature range, the mobility and resistivity of the CdSe/CdTe device vary between μ: $(1.75 \pm 0.45) \times 10^{-3}$ cm^2/V s and (0.27 ± 0.04) cm^2/V s and ρ: $(5.65 \pm 0.15) \times 10^6\ \Omega$ cm and

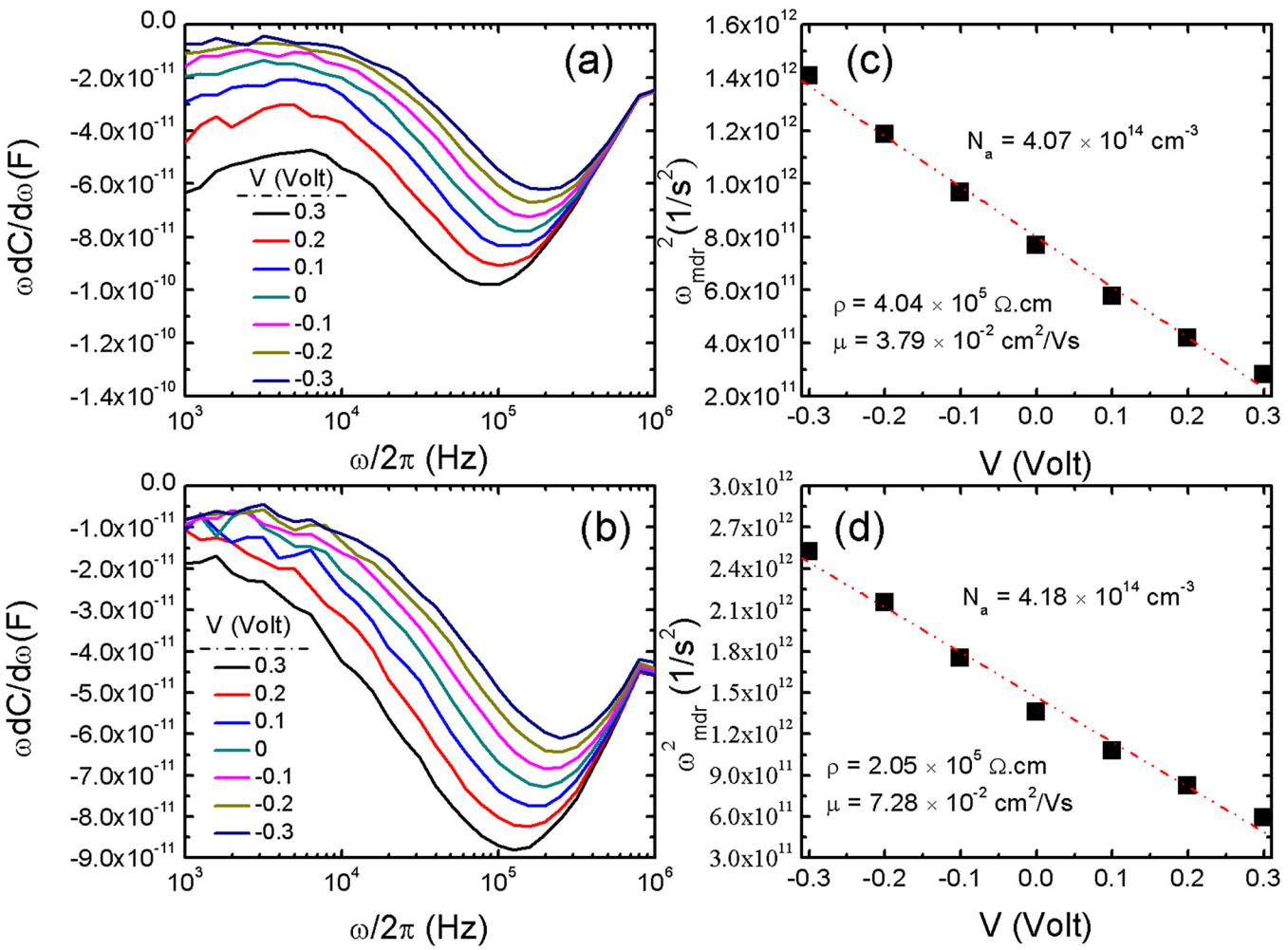

FIG. 5. Differential capacitance spectra in the CdTe solar cell via AS study with two different absorbers [CdS (a) and CdSe (b)] as a function of V to find the values of inflection frequency (ω_{mdr}). The ω_{mdr}^2 vs V plots [CdS (c) and CdSe (d)] are used to extract the hole mobility from the slope (dotted lines are linear fit). The temperature used in this analysis is 104 K.

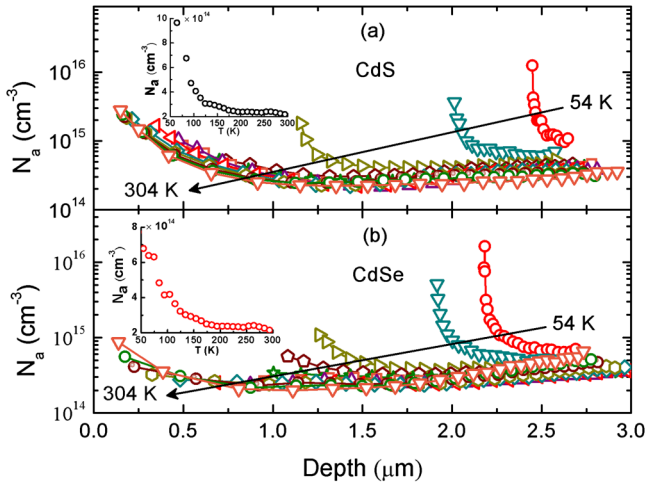

FIG. 6. Temperature dependent CV profiles for CdTe/CdS (a) and CdTe/CdSe (b) devices to extract the carrier concentration (N_a) and their temperature dependence (inset). The frequency used in this extraction is $\omega = 62.8$ kHz. Note that the temperature dependent N_a values will be used in the temperature dependent resistivity and mobility in both devices.

$(7.03 \pm 0.09) \times 10^5\ \Omega$ cm. The observed temperature dependent mobility and resistivity trends are similar to previous reports for a polycrystalline CdTe material.[34,35] We note that in the temperature range of Fig. 8, the mobility and resistivity follow the Arrhenius dependence, $\mu \sim \exp(-E_{a,\mu}/k_BT)$ and $\rho \sim \exp(E_{a,\rho}/k_BT)$, where $E_{a,\mu}$ and $E_{a,\rho}$ are the activation energies of the mobility and resistivity, respectively, as shown in Fig. 9. The extracted activation energies of mobility are 101.2 ± 2.5 meV and 84.7 ± 2.7 meV for CdS/CdTe and CdSe/CdTe devices, respectively. Similarly, the extracted activation energies of resistivity for CdS/CdTe and CdSe/CdTe devices are 92.6 ± 3.3 meV and 77.6 ± 4.5 meV, respectively. Comparative activation energies are shown in Table I.

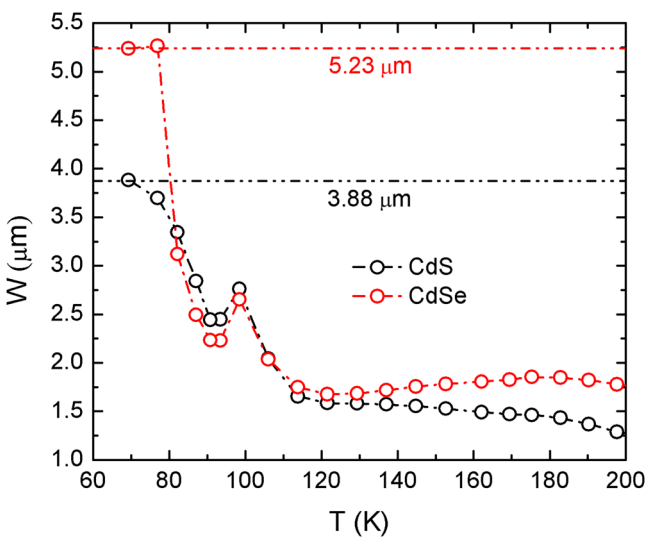

FIG. 7. Temperature dependent depletion width in CdTe solar cells with CdS and CdSe buffers. The absorber widths in these two solar cells were estimated in the completely freeze-out region (dotted horizontal lines represent the absorber width) and are 3.88 and 5.23 μm for CdS and CdSe absorbers, respectively. The frequency and bias in these plots are $\omega = 62.8$ kHz and $V = 0$ V.

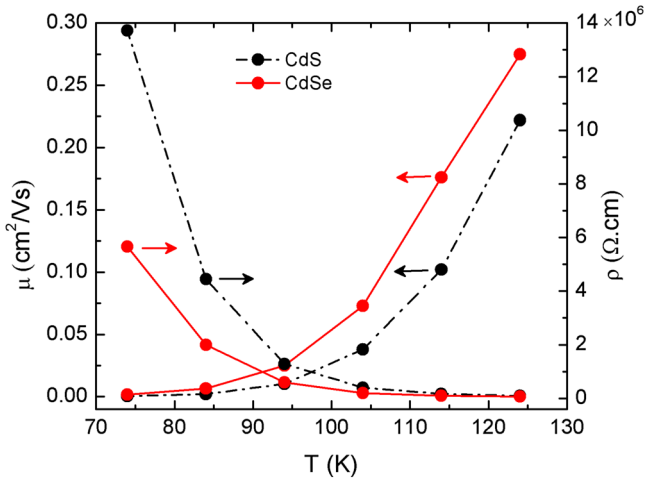

FIG. 8. Temperature dependent mobility and resistivity in CdTe solar cells with two different buffers (CdS and CdSe).

The polycrystalline semiconducting materials consist of variable sized grains and defective grain boundaries which has a significant impact on the energy band and consequently for p-type semiconductors downward band bending occurs and leads to a potential barrier.[17,36–38] This potential barrier hinders the motion of holes in the valence band. So, the activation energies of mobility and resistivity in our CdTe absorber can be representative of grain boundary barrier height in samples due to its polycrystallinity. Previous studies reported the presence of charged grain boundaries in CdS/CdTe solar cell devices and estimated a grain boundary height in the range 90–200 meV.[39,40] In these studies, authors have used different techniques such as Kelvin Probe Force microscopy[39] and temperature and intensity dependent charge transport to estimate the grain boundary height.[40] Vigil-Galán *et al.*[40] estimated the grain boundary height from slope using the $\ln(I \cdot T^{1/2})$ vs $1/k_BT$ plot. Accordingly, if we use $\ln(\mu \cdot T^{1/2})$ vs $1/k_BT$ plots (data now shown), then we get the mobility activation energies 104.5 ± 2.5 meV and 86.9 ± 2.4 meV for CdS/CdTe and CdSe/CdTe, respectively. Similarly, using the $\ln(\rho \cdot T^{-1/2})$ vs $1/k_BT$ formula, we estimate that the activation energies of resistivity for CdS/CdTe and CdSe/CdTe devices are 94.1 ± 1.9 meV and 81.9 ± 4.4 meV, respectively. Our extracted activation energies are consistent with reported grain boundary height range and indicated that the potential barrier height can be a strong factor for the observed temperature dependence of mobility and resistivity in the temperature range 74–124 K. We also note that activation energies of mobility and resistivity for the CdSe/CdTe device are lower (~16 meV) than the CdS/CdTe device. This can be attributed to the difference in the grain boundary barrier height as a function of grain size.[40]

The back-contact barrier in the CdTe solar cell is a serious issue that affects the current–voltage characteristics by impeding hole transport. This limiting effect is commonly referred to as a "rollover" and results in open-circuit voltage and fill factor loss. Figure 10 shows the temperature dependent (T: 70–300 K) current–voltage (JVT) characteristics for (a) CdS/CdTe and (b) CdSe/CdTe solar cells measured in dark.

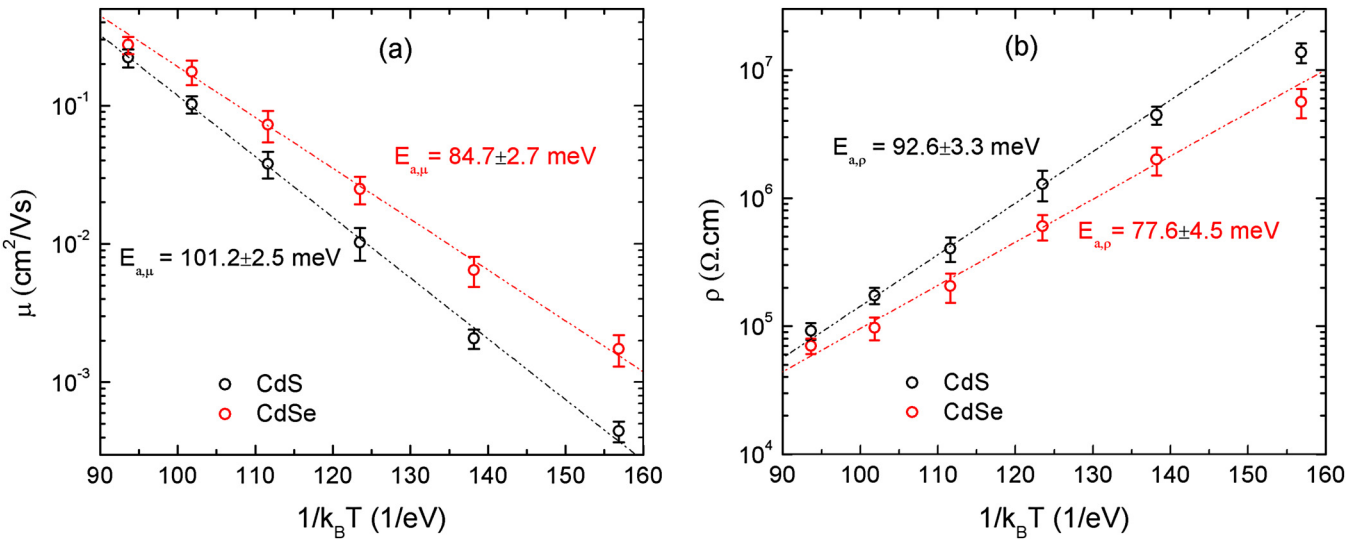

FIG. 9. Arrhenius plots of temperature dependent hole mobility (a) [$\ln(\mu)$ vs $1/k_BT$] and resistivity (b) [$\ln(\rho)$ vs $1/k_BT$] to estimate the mobility and resistivity activation energies in CdTe solar cells with CdS and CdSe buffers.

These results serve as a useful correlated experiment (admittance spectroscopy) to identify the secondary potential barrier due to the back contact.[41]

As seen in the JVT curves (Fig. 10) at large forward bias ($V > 0.6$ V), the front junction (CdS/CdTe or CdSe/CdTe) current density drops off due to the limiting effect of the back-contact barrier. The effect is usually explained by thermionic emission[42] and the current density through absorber/back-contact interface expressed by the Richardson-Schottky formula[43] from which the saturation current density ($J_{0,b}$) can be written as

$$J_{0,b} = A^* T^2 e^{-(\phi_{bc}/k_B T)}. \quad (2)$$

Here, A^* is the effective Richardson constant and ϕ_{bc} is the back-contact barrier height. The back-contact potential barrier height extracted from the $\ln(J_{0,b}T^{-2})$ vs $1/k_BT$ plots, shown in Fig. 11, are 294.6 ± 5.1 meV and 329.4 ± 8.3 meV for CdS and CdSe buffers, respectively (comparison also in Table I). These results are in good agreement with the values 302.1 ± 4.8 meV (CdS) and 321.5 ± 8.6 meV (CdSe) observed via admittance spectroscopy (Fig. 3). The back-contact barrier height has a significant impact on the open-circuit voltage and the fill factor.[44] The higher values of the back-contact barrier in the CdSe/CdTe device could be one of the contributing reasons the $V_{OC} = 0.690$ V and fill factor (FF) = 64.8% are lower than the CdS/CdTe device (V_{OC} = 0.847 V and FF = 70%).

To understand the dominant recombination mechanism [recombination via defect, i.e., Shockley–Read–Hall (SRH) type], we also briefly present a recombination analysis for both cells using previous reports.[45,47] The characteristic

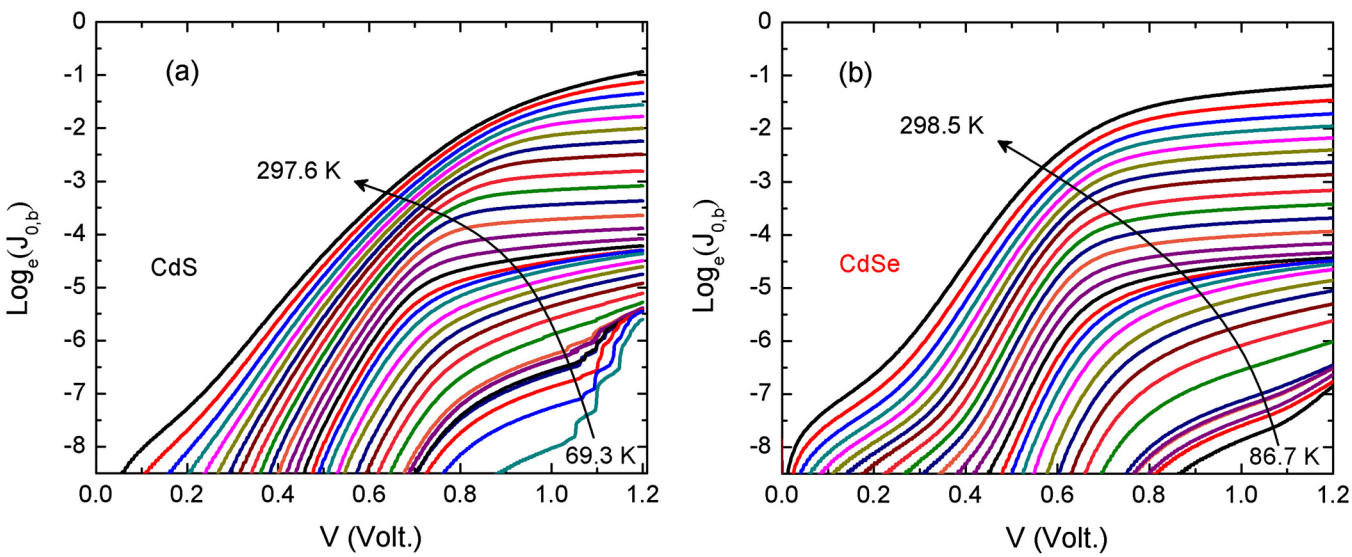

FIG. 10. Temperature dependent (T: 70–300 K) dark current density ($\log_e J_{abs}$) vs voltage (V) characteristics for devices with (a) CdS buffer and (b) CdSe buffer—clear signature of rollover features in both devices above $V > 0.6$ V.

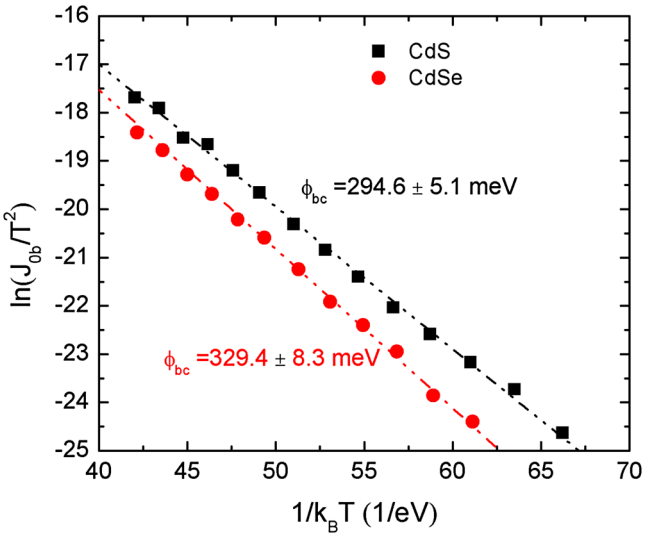

FIG. 11. Arrhenius plot [$(J_{0,b}T^{-2})$ vs $1/k_BT$] to extract the activation energies (φ_{bc}) which is the estimation of back-contact barrier height in CdTe solar cells using CdS and CdSe buffers. The temperature dependent $J_{0,b}$ values were extracted from the rollover feature as seen in the JVT curve [Figs. 10(a) and 10(b)].

recombination activation energy (E_a) is given by $E_a = ((R_0^b E_g + R_0^I \varphi_{b0})/(R_0^b + R_0^I))$. Here, R_0^b and R_0^I are the bias (either electrical or optical) independent SRH recombination rates. E_g and φ_{b0} are the bandgap and potential barrier for the majority carrier at the buffer/absorber interface, respectively. The recombination activation energy (E_a) is then expressed as the average of E_g and φ_{b0} weighted by respective recombination rates R_0^b, and R_0^I—i.e., the effective energy gap across which the carriers recombine. The temperature dependence of V_{OC} (under one sun) for both cells is shown in Fig. 12(a). At higher temperatures, V_{OC} decreases linearly with temperature. In this region, the CdS-buffered device exhibits a higher V_{OC} than the CdSe-buffered device. The extrapolated values of E_a are 1.38 and 1.29 eV for CdS- and CdSe-buffered devices, respectively (Table I). The extrapolated E_a value is a measure of maximum attainable quasi-Fermi level separation. If E_a equals the absorber bandgap, then V_{OC} is dominated by the bulk recombination. On the other hand, for E_a value smaller than bandgap, one expects a significant portion of the total recombination to occur at the interfaces. The bandgap of the CdTe absorber is ~1.5 eV. We conclude that the observed E_a value (1.38 eV) implies that the bulk recombination in CdS/CdTe device is dominating. It was reported that the reduction of absorber bandgap in the CdSe/CdTe device is due to Se diffusion.[9] According to the bandgap estimation method from the absorption edges in external quantum efficiency spectra reported by Helmers *et al.*,[48] the bandgaps of the $CdTe_xSe_{1-x}$ alloys are found to be a strong function of CdSe window layer thickness (for example, the reduction of bandgap from 1.475 to 1.354 eV with the increase of CdSe thickness 0 and 750 nm, respectively).[11] Also, with a 100 nm CdSe window layer, a 0.055 eV reduction in bandgap was observed from the standard CdS/CdSe cell by Paudel and Yan.[11] The spectral photoluminescence data, shown in Fig. 12(b), show the bandgap reduction of 0.06 eV in the CdSe/CdTe ($E_g = 1.40$ eV) device from the CdS/CdTe ($E_g = 1.46$ eV) device (noted in Table I).

The reduction in bandgap in the CdSe/CdTe-based solar cell, compared to the CdS/CdTe case, is consistent with the lower recombination activation energy (1.29 eV) observed in this work. While CdSe is more likely than CdS to have a conduction band edge energetically lower than that of CdTe, and while this presents less of a barrier for interfacial recombination of electrons, by forming a clifflike rather than a spikelike conduction band offset,[49] the temperature dependent analysis of V_{OC} suggests instead that bulk recombination is dominant. We note that progress has been made to effectively reduce the V_{OC} deficit in selenide-containing devices by adding[50,52] appropriate oxide buffers, also called the "high-resistance transparent" (HRT) layers, between the

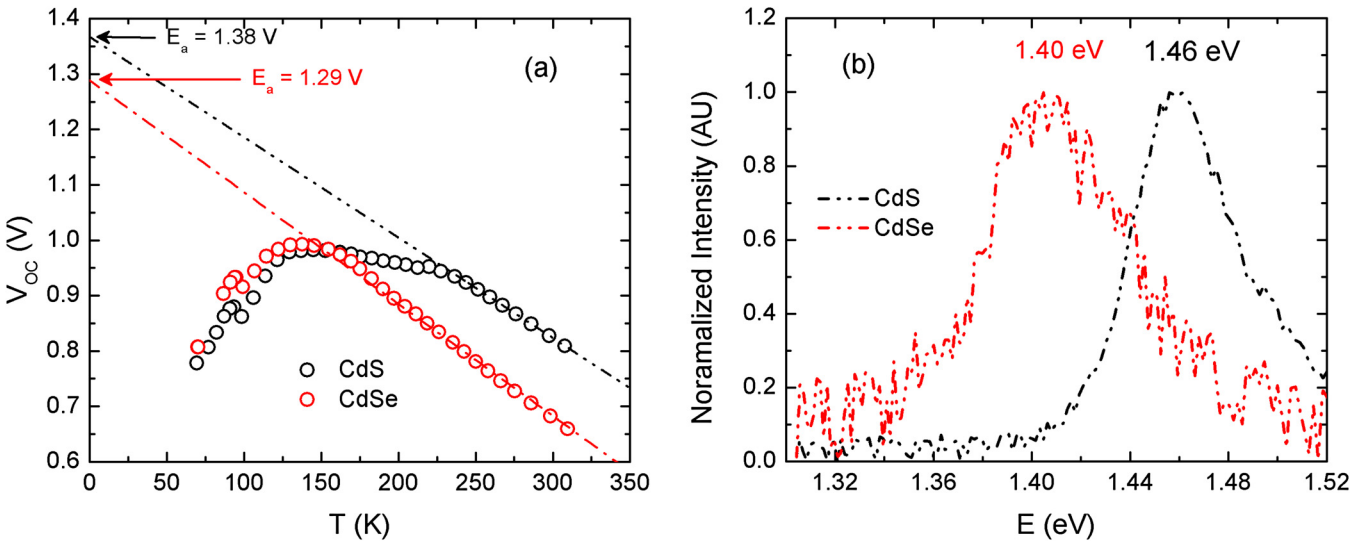

FIG. 12. (a) Temperature dependent open-circuit voltage (V_{OC}) in CdTe solar cells with CdS and CdSe buffers (under 1-sun illumination). The solid lines represent the linear extrapolation to $T = 0$ K that reveals the dominant recombination process. (b) The spectral photoluminescence data (normalized) for the CdTe solar cells with CdS and CdSe buffers show the optical bandgap of 1.40 eV (CdSe) and 1.46 eV (CdS), respectively.

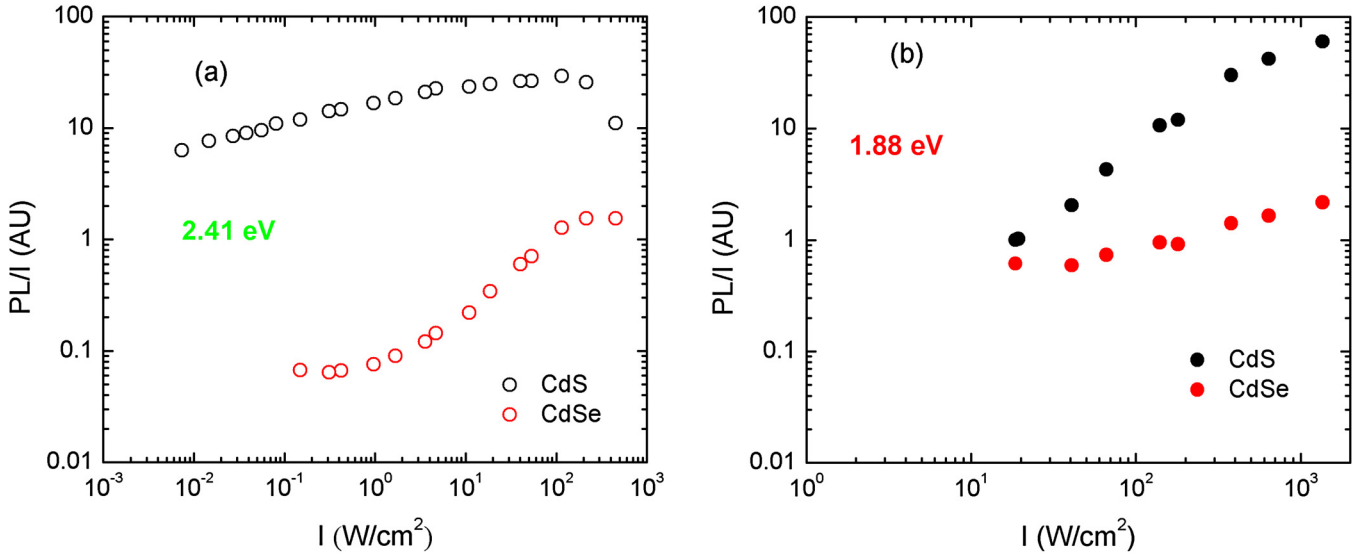

FIG. 13. PL intensity divided by excitation intensity (PL-I) is shown as a function of excitation intensity for CdTe solar cell with two different buffers (CdS and CdSe). The excitation energies used are (a) 2.41 eV and (b) 1.88 eV.

transparent conductive oxide (TCO) and CdSe (or CdS) buffer. This layer may function to promote the formation of a spikelike compound interface of TCO/HRT/CdSe/CdTe, hence improving device V_{OC}. Because the n-type TCO/HRT/CdSe stack is much more heavily doped and electrically thinner than the p-type absorber, any defects at the TCO/HRT or HRT/CdSe interface would contribute a relatively subdued signal to the overall device capacitance. We do not regard the signatures observed in this study as being associated with the TCO/HRT or HRT/CdSe interfaces.

We further analyze here the recombination that occurs radiatively in both CdS/CdTe and CdSe/CdTe solar cells using PL-I characterization of the polycrystalline samples. Figure 13 shows the measured PL intensity normalized by excitation intensity, which is proportional to radiative recombination efficiency. While the radiative efficiency in the CdSe/CdTe device rises with higher excitation intensity, the heating effect due to the laser illumination is found to cause a drop of PL signal which worsens over the course of several seconds.

The PL-I signal in the CdS/CdTe device is very bright compared to the CdSe/CdTe device. This result was also observed in spectral PL measurements. This can be due to the 2.41-eV excitation for the PL-I measurements being partially absorbed by the CdS layer, and some of the detected PL may originate from defects in the CdS. To overcome the possibility of the luminescence from the CdS counterpart, we also performed the PL-I measurements in these two cells using a lower laser excitation energy, 1.88 eV instead of 2.41 eV. The results suggest that the fairly constant efficiency seen for the CdS/CdTe device in Fig. 13(a) is related to excitation in the vicinity of the CdS layer. The results also confirm that when the excitation of the front layer is minimized, the PL efficiency shown in Fig. 13(b) remains larger in the CdS/CdTe device compared to that of the CdSe/CdTe device, which is consistent with a reduction of photocarrier density caused by the increased defect density detected in the CV and DLCP measurements.

V. CONCLUSIONS

This study combines electrical and optical characterization to gain insight into the properties of CdSe-buffered and CdS-buffered solar cells. The investigations address active defects, transport properties, and recombination in the bulk and interface regions. Carrier density profiles in the CdS/CdTe device, obtained via CV and DLCP, are found to agree with each other. However, there is dissimilarity in the CdSe/CdTe device, which is attributed to the presence of defects in the bulk of the CdTe absorber. Differential capacitance versus temperature spectra shows two defect signatures for each sample at low and high temperature. For both devices, defects associated with the low- and high-activation energy are related to the freeze-out of the CdTe absorber and the presence of a nonohmic back-contact, respectively. Defect energies extracted from the admittance spectroscopy (CdS: 302.1 ± 4.8 meV and CdSe: 321.5 ± 8.6 meV) and JVT (CdS: 294.6 ± 5.1 meV and CdSe: 329.4 ± 8.3 meV) measurement are in good agreement. The temperature dependence of mobility and resistivity in both cells shows activation energies of mobility [$E_{a,\mu}$: 101.2 ± 2.5 meV (CdS buffer) and 84.7 ± 2.7 meV (CdSe buffer)] and resistivity [$E_{a,\rho}$: 92.6 ± 3.3 meV (CdS buffer) and 77.6 ± 4.5 meV (CdSe buffer)] are related to the band fluctuation or grain boundary barrier height. PL-I measurements, which are sensitive to nonradiative recombination, show much lower radiative efficiency in the CdSe/CdTe cell which is attributed to higher energy defects.

ACKNOWLEDGMENT

The authors acknowledge support from the U.S. Department of Energy through Sunshot PVRD Grant No. DE-EE-0007541 "Crosscutting recombination metrology for expediting V_{OC} engineering."